Nuclear Engineering and Design 460 (2026) 115270



Contents lists available at ScienceDirect

Nuclear Engineering and Design

journal homepage: www.elsevier.com/locate/nucengdes



Benchmarking CAPRIX pin behaviour under irradiation with high plutonium content: comparison with experimental data

M.-M. Desagulier [a,*], D. Jaramillo-Sierra [b,c], B. Burger [d], L. Argeles [e], M. Stefanowska-Skrodzka [f], J. Lavarenne [f], V. Dupont [a], E. Deveaux [a], A. Del Nevo [c], E. Brunetto [g], A. Scolaro [g], J. Gado [d], K. Sturm [h], A. Rineiski [h], L. Luzzi [b], A. Magni [b], D. Pizzocri [b], K. Mikityuk [i], A. Jiménez-Carrascosa [i], S. Lemehov [j], V. Matocha [k], S. Bebjak [l], C. Strmensky [l], V. Blanc [a], N. Chauvin [a]

[a] Commissariat à L'énergie Atomique et aux Énergies Alternatives – Cadarache, 13108 Saint-Paul-lez-Durance, France
[b] Politecnico di Milano, Department of Energy, Nuclear Engineering Division, via La Masa 34, 20156 Milano, Italy
[c] ENEA, NUC-ING, Località Bacino del Brasimone 1, Camugnano, 40032 Bologna, Italy
[d] EK-CER, 1-3 Konkoly-Thege Miklós út, 1121 Budapest, Hungary
[e] EDF, Lab R&D Renardières, MMC, 4 Avenue des Renardières – Ecuelles, 77250 Moret sur Loing et Orvanne, France
[f] Jacobs, Kings Point House, Queen Mother Square, Poundbury, Dorchester DT1 3BW, UK
[g] École Polytechnique Fédérale de Lausanne, Route Cantonale, 1015 Lausanne, Switzerland
[h] Karlsruhe Institute of Technology, Hermann-von-Helmholtz-Platz 1, 76344 Eggenstein-Leopoldshafen, Germany
[i] Paul Scherrer Institute, Forschungsstrasse 111, 5232 Villigen, Switzerland
[j] Belgian Nuclear Research Centre SCK·CEN, Boeretang 200, 2400 Mol, Belgium
[k] Ústav Jaderného Výzkumu Řež, Hlavní 130, 250 68 Husinec-Řež, Czech Republic
[l] VUJE, Okružná 5, 918 64 Trnava, Slovakia

ARTICLE INFO

Keywords:
Fuel performance codes
Benchmark
Prediction
Experiment
Comparison
Behaviour

ABSTRACT

This paper presents the results of the second phase of the benchmark exercise in the Plutonium Management for More Agility project (PuMMA), which aims to enhance the reliability of fuel performance codes (FPCs) for Mixed Oxide (MOX) fuels with high plutonium content. This phase involved the simulation of the CAPRIX irradiation (45% of Pu) carried out in the PHENIX reactor in France. Thirteen organizations from nine countries participated, using eight different fuel performance codes. In this phase, 7 codes then improved its modelling by optimizing parameters and/or improving the formulation of some models involved in the computation. A comparative analysis was then conducted between the codes and the post-irradiation experimental (PIE) results, with the objective of identifying the improvements made, the discrepancies still observed, and to define future areas for improvement and development. The present paper demonstrates the results for the CAPRIX pin.

The main results despite the discrepancies noted between the codes and/or with the experimental data, the work carried out through this benchmark has demonstrated the capacity of the codes to optimise/improve their simulation in order to approximate the PIE. Moreover, the methodology employed yielded a comprehensive and precise analysis, thus facilitating the suggestion of approaches to the development of specific models. This finding thus demonstrates the potential of fuel performance codes modelling pins with high Pu contents.

1. Introduction

Uranium and Plutonium mixed oxide fuels are a leading fuel for Sodium Fast Reactors (SFR). The plutonium fraction and the Oxygen/Metal ratio (O/M with M = U + Pu) specifications must range between 0.20 and 0.35 (Pu / (U + Pu)) and $1.94 \leq O/M < 2.00$, respectively. From the last century, research into actinide transmutation was one of the European waste management R&D areas. This way, new non-conventional fuels are studied in the frame of European and International collaboration. In this context, the CAPRA program (Consommation Accrue de Plutonium dans les RApides) (Languille et al., 1998), underway at CEA, started. The objective is to assess the feasibility of a Fast

* Corresponding author.
E-mail address: marie-margaux.desagulier@cea.fr (M.-M. Desagulier).

https://doi.org/10.1016/j.nucengdes.2026.115270
Received 7 April 2026; Received in revised form 1 October 2026; Accepted 6 October 2026
Available online 16 October 2026
0029-5493/© 2026 The Authors. Published by Elsevier B.V. This is an open access article under the CC BY license (http://creativecommons.org/licenses/by/4.0/).

Reactor optimised to burn as much plutonium as possible but which also contributes to the destruction of minor actinides. To achieve an attractive plutonium burning rate, high Pu content is needed. The maximum amount of Pu on mixed oxide was defined at 0.45, to ensure the compatibility with the dry route fabrication process and PUREX (Plutonium, Uranium, Reduction, EXtraction) process reprocessing (Herbst et al., 2011). This kind of fuel, with high Pu content offers significant potential for safer, more efficient and sustainable nuclear energy production. It is also a challenge, to understand the complexities associated with high Pu content MOX fuels in fast reactors (FRs). This is essential for enhancing the readiness level of this technology as well as ensuring optimal safety and performance. In this work, the simulation under irradiation of CAPRA fuel is studied (45% of Pu). Most specifically, one CAPRIX pin, composed of CAPRA pellets, irradiated in the PHENIX reactor from January 1995 to January 2006 is studied. As part of the PuMMA (Pu management for more agility) project, PIE were performed on the CAPRIX pin. These experimental data are detailed in (Fayette et al., 2026). Most specifically, within the PuMMA project the aim of Working Package 2 is to study the behaviour of fuel in FRs under high Pu content conditions. This benchmark study involves the use of various FPCs to extend their validity domain by simulating the three fuel pins (CAPRIX, TRABANT1 and TRABANT2), whose irradiation experiments specifications are available in (Jaramillo-Sierra et al., 2025b). It is divided into two phases:

- **Code-to-code comparison**: This initial phase, detailed in (Jaramillo-Sierra et al., 2025b), permits to identify the main variations between the different codes, and to investigate the sources of discrepancies. This analysis highlights which models and correlations contribute most to the observed variations, guiding improvements for the second phase (presented in this paper).
- **Experimental data comparison**: The second phase validates the FPCs against experimental data obtained from PIEs of the fuel pins.

Subsequent to the initial phase, a comprehensive investigation was undertaken to identify the primary variations between the various codes, the origins of these discrepancies, and a complementary sensitivity analysis was conducted (Jaramillo-Sierra et al., 2025b). The initial analysis revealed which models and correlations contributed most to the observed variations, thereby guiding improvements/assessments for the subsequent phase. The second phase, as outlined in this study, involves a comparison between PIE data and calculated data derived from codes. The present study will make use of seven different FPCs in order to draw comparisons between them. The simulation time was extended from the end of the irradiation to the PIE time. For the CAPRIX pin, the focal point of this study, a PIE time of 9325.9 days was assumed. The inclusion of the storage period in the simulated histories was found to be a valuable method for accounting for the helium production by α-decay during the storage period. This choice was adopted with the objective of obtaining more representative predictions of the final composition and pressure of the plenum gas, which could then be compared to the puncturing results.

A uniform comparison of all code results with the experimental data was conducted to identify which code exhibited the lowest discrepancy with the experimental data for each physical quantity of interest. It is evident that, by employing this methodology, the optimal correlations and settings for simulating high Pu MOX behaviour have been identified.

2. The CAPRIX irradiation in the PHENIX reactor

This section provides a detailed description of the irradiation experiments considered in this benchmark, outlining their specifications and relevance to the extension of the validation of FPCs. Table 1 provides a concise overview of the key specifications of the irradiation experiments that form the subject of this study. The selection of experiments was based on three criteria: high Pu content, relevant irradiation conditions, and the availability of high-quality PIE data. The latter is essential for the validation of models and integral codes.

Table 1
CAP01 pin irradiation experiments specifications.

Pin specifications	Unit	CAPRIX
Reactor		PHENIX (FR)
Equivalent irradiation time	days	359.8
Max. LHR	W/cm	354.2
Max. Cladding temperature	K	750
Max. Burnup	% FIMA	12.8
MOX fuel composition		$U_{0.55}Pu_{0.45}O_{2.00}$
Manufacturer		JRC (Joint Research Centre)
Active length	mm	850
Fuel central hole diameter	mm	2.0
Fuel pellet diameter	mm	5.42
Initial gap	mm	0.115
Total porosity	%	5.47
Cladding		AIM1
Cladding outer diameter (OD)	mm	6.55
Cladding inner diameter (ID)	mm	5.65
Filler gas pressure (at room temperature 20 °C)	Bar	1
Filler gas composition	%	He: 95 N_2: 5

The CAPRIX irradiation was conducted in the PHENIX reactor from January 1995 to January 2006. The CAPRIX1 capsule contained two experimental pins (CAP01 and CAP02) and 17 standard PHENIX pins. The CAP01 pin was irradiated from the 49th to the 53rd cycle, for a period of approximately 360 equivalent full power days (EFPD).

A complete set of specifications was provided to all participants, encompassing the fuel and cladding geometries and properties, as delineated in Table 1. It is noteworthy that each participant employed the same set of input data. The boundary conditions provided are as follows: Linear heat rate (LHR), neutronic flux and the cladding external temperature. These boundary conditions were supplied at every time step and axial position (Venard and Deveaux, 2021). More specifically, the characteristic quantities of the irradiation (neutron flux, linear heat rate, clad irradiation damage, burn-up, cladding temperature profiles at the median fiber and external clad temperature) were realized with the Monte Carlo code TRIPOLI4 (TRIPOLI-4® Project Team, 2015) and the thermal-hydraulic code TRIO MC (Gerschenfeld and Gorsse, 2022).

For instance, Fig. 1 illustrates the linear power rate and the cladding temperature at the peak power node of the CAPRIX pin, utilised as the input data. With regard to the fundamental nuclear data, this is available in the JEFF 3.1 nuclear data libraries (NEA (Nuclear Energy Agency), 2026).

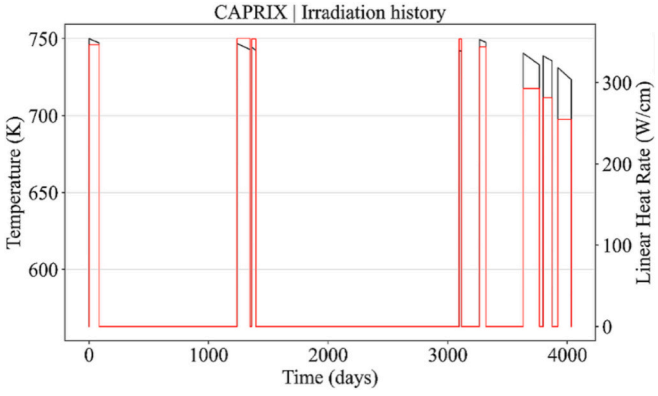


Fig. 1. CAPRIX Cladding nominal temperature (black line) and linear heat rate (red line) at the peak power position. (For interpretation of the references to colour in this figure legend, the reader is referred to the web version of this article.)

3. Method

3.1. Experimental data available for comparison

The CAPRIX1 capsule contained two experimental pins (CAP01 and CAP02) and 17 standard PHENIX pins. Subsequent to the irradiation, non-destructive examinations were conducted at the "Cellule des Eléments Irradiés" (CEI) of PHENIX from 2006 to 2008. The two experimental pins were transported to the LECA hot cell facility in Cadarache at the end of 2019 with the objective of conducting additional non-destructive examinations, cutting and destructive examinations. As illustrated in Table 2, a range of non-destructive and destructive PIE procedures were conducted on the CAP01 pin. The majority of the results presented in this table were utilised for the purpose of experimental/calculation comparison and will be discussed in this paper.

3.2. Fuel performance codes improvement

The second phase of the benchmark exercise involved the efforts of 14 European organizations, including seven FPCs: The following institutions are involved in the project: FEMAXI (Karlsruher Institut für Technologie – KIT), FRED (Paul Scherrer Institut - PSI), FUROM (Energiatudomanyi Kutatokozpont - Centre for Energy Research - EK-CER), GERMINAL (Commissariat à l'énergie atomique et aux énergies alternatives - CEA, Électricité de France - EDF and Franco-américaine de constructions atomiques - FRAMATOME), MACROS (Studiecentrum voor kernenergie Centre d'étude de l'énergie nucléaire SCK CEN), OFFBEAT (Ecole polytechnique fédérale de Lausanne - EPFL) and TRANSURANUS (European Nuclear Energy Agency - ENEA, Politecnico di Milano - POLIMI, Nuclear Research Institute Rez - UJV and Nuclear Power Plant Research Institute - VUJE). When several entities performed the calculations using the same code, they worked together to improve the calculations during Phase 2. For a comprehensive overview of the codes, please refer to (Jaramillo-Sierra et al., 2025b), which provides a detailed description of Phase I of this exercise. The codes represent a 1.5D axisymmetric domain, while some have the capability to extend to 2D and 3D simulations (i.e. OFFBEAT). This section delineates the alterations made to the modelling between phase 1 (Jaramillo-Sierra et al., 2025b) and phase 2, for each code:

- **FEMAXI (KIT)**: The tooling modernization for sensitivity analyses was performed. For detailed burn-up analysis to accurately predict Helium and fission gas production, chaining of C4P-TRAIN and FEMAXI was realized. This preliminary version of explicit on-line coupling provides radial depletion profiles. Then, power-level based activation of Helium release from fuel matrix to plenum to better predict pin pressure was also performed. Finally, a fuel melting correlation was added.
- **FRED (PSI)**: Two main modifications were made in the FRED code. A new numerical library was implemented to improve the time integration stability. And MOX fuel swelling rate model was modified to introduce a calibration multiplier.
- **FUROM (EK-CER)**: No significant changes were carried out between the first and second phases of comparisons. However, several minor corrections were made. Axial deformations were calculated only for the active part of the fuel, taking into account only the volume of the plenum. As the total pin length was given as an experimental result, the FUROM results were corrected by taking into account the total cladding length, not only the length of the active part. In FUROM code the restructured zone is the zone of re-crystallization that was not measured in PIE. On the other hand, FUROM does not calculate the size of the high burnup zone that is considered to be the restructured zone in PIE studies. Therefore, FUROM data related to the restructured zone were deleted.
- **GERMINAL**: the newest version of GERMINAL (GV2.2.5) was used for the calculations. First, the irradiation history was modified. On the phase 1 of the benchmark (Jaramillo-Sierra et al., 2025b), an average linear power value was taken into account for each irradiation cycle. The improvement was to consider the right value at the beginning and at the end of the irradiation cycle. The thermal conductivity empirical law is the Philipponneau law by default in Germinal simulation (Philipponneau, 1992). But for the improvement of our calculation, the EGIFE recommendations was used, corresponding to Kato's recommendation (NEA (Nuclear Energy Agency), 2025). The JOG (Joint Oxyde Gaine) model was activated to take into account the closure or not of the gap. The thickness of the dense JOG is determined by the uniform spreading of the volume of volatile fission products released onto the inner surface of the cladding. A threshold temperature was defined for the He release, close to the storage temperature. This way, below this temperature, there is no helium release. This stabilises the release of He during the storage. Then, addition of 1 time step per year of storage were added in order to provide a more representative storage period.
- **OFFBEAT**: On the one hand, several MOX fuel properties were updated. The thermal expansion from the MATPRO model to Lemehov's correlation, as outlined in INSPYRE D7.2 (Van Uffelen et al., 2025). This change reflects a more recent and experimentally validated description of MOX thermal expansion behaviour, enhancing predictive accuracy, especially at higher temperatures. The Young's modulus correlation was also updated: from MATPRO to Lemehov's correlation (INSPYRE D7.2) (Van Uffelen et al., 2025). This adjustment provides a more precise characterization of MOX fuel's elastic properties, particularly in high-temperature regimes, improving the accuracy of deformation predictions during irradiation. Then the the Routbort-Combette MOX fuel creep model was incorporated (Routbort et al., 1972; Combette et al., 1977). Previously modeled as purely elastic, the fuel now accounts for time-dependent deformation, offering a more realistic assessment of long-term performance. On the other hand, an optimization of the meshing was also performed. Progressive grading towards the pellet centerline was chosen, this permit to increase resolution and enhance the accuracy of these critical effects.
- **TRANSURANUS**: The model that consistently describes fission gas release and gaseous swelling by modelling bubble behaviour both within the grains and along the grain boundaries was used. This model enables the capture of the relationship between fission gas swelling, release, and their dependence on local hydrostatic stress in the fuel (Pastore et al., 2013). The mechanistic treatment of fission gas release also permits the implementation of the burst release model (Pizzocri et al., 2015). Also, the number of fuel cracks was modeled as a function of the linear heat rate (Bruschi and Barani,

Table 2
PIE data available on CAPRIX (CAP01) pin (Jaramillo-Sierra et al., 2025b).

Type of measurement	Output
Length measurement	Cladding length Cladding relative growth
Neutron radiography	Fuel column length
Gamma spectrometry	Radio nuclide distribution
Laser shadowgraphy	Cladding outer diameter
Irradiation data	Axial burn-up (BU) Plenum gas pressure (Xe + Kr) produced and released
Puncturing and fission gas analysis	Xe, Kr produced and released Plenum gas composition (He, Xe, Kr)
Density measurements	Density
Macrograph studies dimensional measurements	Central hole diameter Restructured thickness Pellet outer diameter Fuel-cladding gap Cladding inner and outer diameter
Element's redistribution	Matrix and fission products

2015). The Young's modulus correlation considered on the calculation combines dependencies on stoichiometry, burn-up, porosity, and initial Pu content taking into account the local fuel temperature. This correlation was fitted to molecular dynamics calculations and validated with experimental data (Lemehov and Cen, 2020; Balboa et al., 2017). Finally, the fuel-cladding gap conductivity model used is based on ESFR-SMART results with two variables, fuel rating and burn-up (Lavarenne et al., 2019).

- **MACROS**: Only the gap conductance model (GCM) was modified. A new model was used. This is a modified version of well-known Offset Gap Conductance (OGC) model from the code FRAP-T6. The distance pellet-cladding changes (circumferentially) is taken into account. The gap is divided in a number of circumferential segments (9 by default).

In addition to these elements, the reference material laws used for each of the performance calculation codes are summarised in the appendix to the sensitivity analysis (Jaramillo-Sierra et al., 2025b). However, some models and correlations could not be retrieved due to limited data sharing.

4. Benchmark results

This section is dedicated to the presentation of a comparative analysis between the simulation and the post-irradiated experimental results. In order to ensure clarity, post-processing choices were made. Specifically, the simulated value is shown to correspond to the time step of the end of storage, at 9325.9 days. To facilitate the identification of whether the calculated values were more or less distant from the experimental value, a colour code was employed. In instances where the calculated values lay within the range of $+/-$ 1ε or $+/-$ 2ε (where ε corresponds to the measurement uncertainty, which is the one shown in the graphs), they were designated in green or yellow, respectively. Finally, if the calculated value was outside the range of $+/-$ 2ε, it was identified in red. In instances where a substantial deviation was observed, extending beyond the established order of magnitude, the value was accentuated in bold red. This methodological approach guarantees a more uniform comparison among the codes and with the experimental data.

In certain cases, temporal evolutions of specific values are presented. In order to ensure the comparisons are more representative, the curves calculated by all participants were drawn over the entire irradiation period with the storage period (colored curves), and the experimental data corresponds to the black dot. In this section, the comparison is followed by a critical analysis of the observed discrepancies. The analysis is divided into two sections, corresponding to the two scales of the experimental study: the pin scale and the pellet scale. The results of the comparison are then used to establish possible guidelines for model development.

4.1. Pin scale results

Initially, the gas was punctured from the pin following storage, thus enabling the measurement of the volume and composition of fission gas released, at 20 °C and 101,325 Pa. Calculations were performed in order to allow the estimation of the fraction of gas released and the molar fraction of Xe and Kr released. The total produced gases have been calculated with GERMINAL V.2.2.5 fuel performance code. These calculations allow to estimate the fraction of gas released. The quantity of produced gases has also been calculated separately for Xe and Kr with fuel evolution code TRIPOLI 4. The molar fraction of gas released was estimated on the basis of these TRIPOLI 4 calculations and the composition measurement. The gas was found to be composed of 73.4% xenon (Xe) and 5.1% krypton (Kr), with the remainder being helium (He). These values correspond to the PIE values employed for the comparison. The release fractions for xenon (Xe) and krypton (Kr) were estimated by comparing the released gas volume with the produced gas calculation at the end of irradiation.

Firstly, a cross-code qualitative comparison was conducted. The evolution of the fission gas released volume along the irradiation cycle and storage, calculated by all codes, is represented in Fig. 2a. For all codes, the fission gas released volume remains constant during the storage time. Furthermore, throughout the irradiation cycle, the evolution of the released volume demonstrates a consistent trend, with the exception of FUROM (yellow curve). The issue can be attributed to an error during the preparation of the output file. In summary, the purpose of the codes is to compute the quantities of fission gas released. Subsequently, the quantities are converted into a volume using the ideal gas law, with conventionally given values, defined in the code, for T and P being utilised. When intending to compare with the puncturing result at 20 °C, it is imperative that all quantities computed by the codes are converted into volumes at 20 °C and 101,325 Pa. The definition of normal temperature and pressure conditions for each code is given in Table 3, along with the calculated values. A notable observation is the presence of discrepancies, particularly evident in the FEMAXI, FUROM, and GERMINAL codes, where the normal values for temperature or pressure deviate from the measurement conditions. This finding suggests that the values presented may be either overestimated (FEMAXI) or underestimated (GERMINAL, FUROM) in comparison to EPI. Nevertheless, it is important to note that these adjustments would not lead to a different conclusion based on the observations that have already been made. The comparison of the analytical values of the gas composition is illustrated by the histogram in Fig. 2b. For He, as the uncertainty is significant (see grey area corresponding to $\pm\varepsilon$), all the calculated data are in agreement with the PIE value. However, the predicted results are scattered. For Xe, it is evident that only GERMINAL, TRANSURANUS and FEMAXI results exhibit a close alignment with the PIE value. The remaining codes, MACROS, FRED, FUROM and OFFBEAT, demonstrate a disparity in their estimation, with the tendency to either underestimate or overestimate the PIE value, respectively. It is noteworthy that Kr demonstrates a uniform alignment with the PIE value across all codes, with the exception of OFFBEAT, which estimates 10% against a 5% value. These discrepancies could be attributed to the burn-up discrepancy. This point will be explored in the discussion section.

The plenum gas pressure was also studied. Fig. 3 provides a graphical representation of the variation in gas pressure over the complete irradiation cycle and subsequent storage period. With the exception of MACROS, all codes calculated a constant gas pressure during both the storage and the inter-cycles. One of the explanations for this phenomenon is that the uniform temperature measured at the end of the previous irradiation cycle may be equivalent to the reactor temperature without power (400 °C), and the temperature recorded at the end of the storage period is equivalent to the ambient temperature (20 °C). These preliminary responses necessitate further investigation. Therefore, a decrease in pressure is concomitant with a decrease in temperature. FRED also exhibited a similar behaviour during the inter-cycle phase, which is consistent with the observations of inconsistencies in the linear power. Indeed, the linear power during the inter-cycles was not considered to be equal to 0 W.cm-1; rather, it was observed to decrease continuously until it reached zero at the end of the inter-cycle. As demonstrated in Fig. 2, TRANSURANUS, FEMAXI, FUROM and OFFBEAT demonstrate a high degree of agreement, with a maximum discrepancy in pressure estimation of 1%. The remaining codes – FRED, GERMINAL and MACROS – have been found to overestimate the plenum pressure (up to 32%). In relation to the preceding volume measurement, the gas pressure was punctured at 20 °C and 101,325 Pa. It should be noted that these conditions may vary for different codes, as it is details in the Table 3. As with the volume of gas released, the same conclusions can be drawn regarding the internal pressure. Should the calculated values be adjusted to the measurement temperature, it is predicted that GERMINAL would overestimate the internal pressure (17.1 bar) and FEMAXI would underestimate it (11.8 bar). This does not provide any

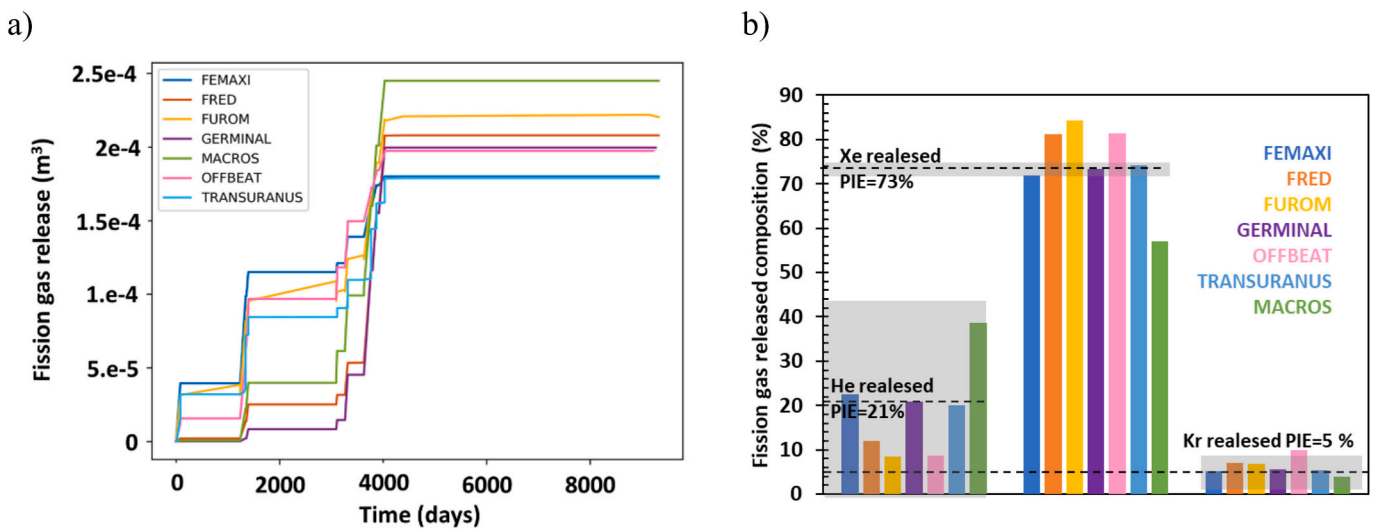


Fig. 2. Comparison of a) the volume released along the irradiation and b) the fission gas released composition calculated with the PIE values.

Table 3
Plenum pressure and total volume released calculated and measured (with green for data within ±1ε, yellow for data within ±2ε and red for data outside ±2ε).

Output	V-2Ɛ	PIE value	V+2Ɛ	FEMAXI	FRED	FUROM	GERMINAL	OFFBEAT	TRANSURANUS	MACROS
		20°C 1 bar		25°C 1 bar	20°C 1 bar	20°C 0.1 bar	0°C 1 bar		20°C 1 bar	
Plenum gas pressure (bar)	12.1	**12.9**	13.7	12	14.6	12.2	16	12.04*	13.3	15.5*
Total gas released cm^3	179.8	**194.6**	209.4	185.3	207.9	199.7	199.6	197.3*	178.8	230*

*No data available.

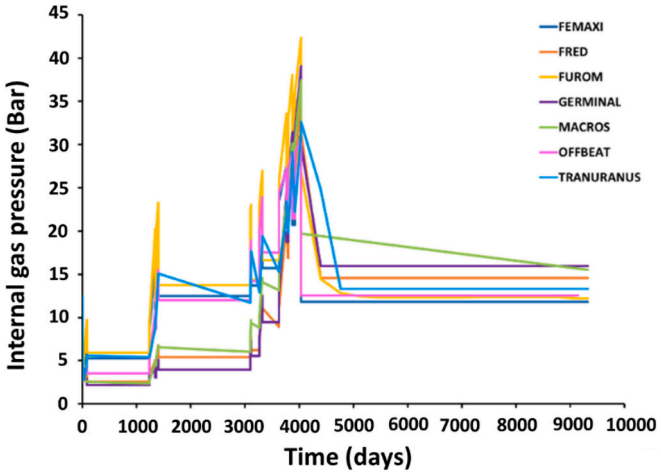


Fig. 3. Internal gas pressure calculated by all codes along the entire irradiation.

additional conclusions.

The initial segment of the study concentrated on the gas data. A notable consistency was observed across the majority of the code predictions, with high internal gas pressure being indicative of a greater volume of gas released. In addition, the Xe/Kr ratios for gas released are fixed by each code and remain constant during the simulation. In view of the constant volumes and pressure during the storage time, it is evident that a potential enhancement to the models could be the incorporation of low linear power and/or low temperature (for instance, during the storage or inter-cycle period).

In the subsequent segment of this section, a comparison of geometric data is conducted, including the cladding and fissile column lengths. The lengths and relative growths of the cladding and fuel column are summarised in Table 4, in comparison to the PIE value. With regard to the fuel column length, it was found that none of the codes were aligned with the experimental data. It is evident from Fig. 4 that all codes overestimated the axial expansion of the fuel column. The closest approximations were GERMINAL and OFFBEAT, with a relative elongation difference of 0.66 and 0.86 above the experimental value (equal to 0.24), respectively. The observed discrepancies can be attributed to the axial fuel relocation model, which requires refinement, and to the way the codes deal with bonding effects between fuel pellets and cladding along the fuel column. It was also highlighted that there is an absence of axial continuity with a 1.5D scheme. This is therefore an intrinsic limitation related to the representation of the pin.

Furthermore, the formation of a bond between pellets and cladding along the column at different axial positions serves to prevent the fuel stack from deforming freely. This results in a shortening of the fuel stack at the end of its operational life. This is the conclusion that was reached in the CAPRIX experiment with regard to the final fuel column length, and the codes do not reproduce the observed behaviour.

In contrast, the cladding length at the end of irradiation, as predicted by all codes, is consistent with the experimental data. The measurements indicate that the elongation of the cladding at the end of its life is very small (only 2 mm compared to its length at the time of manufacture), which is in accordance with predictions made by the relevant codes. However, as illustrated in Fig. 5, there appears to be a discrepancy between the predicted and actual evolutions of the cladding length along

Table 4
Fuel and cladding length calculated by all codes and measured for CAPRIX pin (with green for data within ±1ε, yellow for data within ±2ε and red for data outside ±2ε).

	v-2ε	PIE value	V+2ε	FEMAXI	FRED	FUROM	GERMINAL	OFFBEAT	TRANSURANUS	MACROS
Fuel column length (mm)	849.6	852	854.4	867.6	873.4	863.1	857.7	859.5	866.8	867.45
Relative growth (%)	-0.25	0.235	0.715	2.1	2.8	1.5	0.9	1.1	1.97	2
Clad length (mm)	1792.4	1794.4	1796.4	1793.7	1790.7	1794.5	1793.7	1793.9	1794.1	1794.3
Relative growth (%)	0	0.06	0.18	0.02	-0.15	0.08	0.017	0.28	0.04	0.058

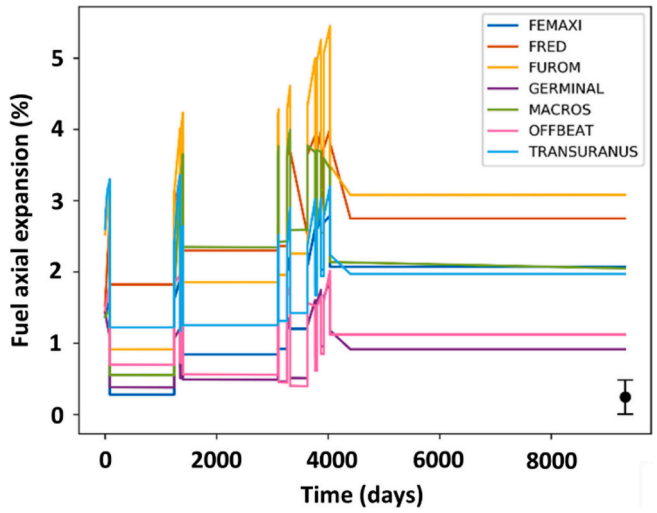


Fig. 4. Fuel column axial expansion along the entire irradiation and storage (colored curves) compared to the experimental data (black dot with experimental uncertainty ±ε).

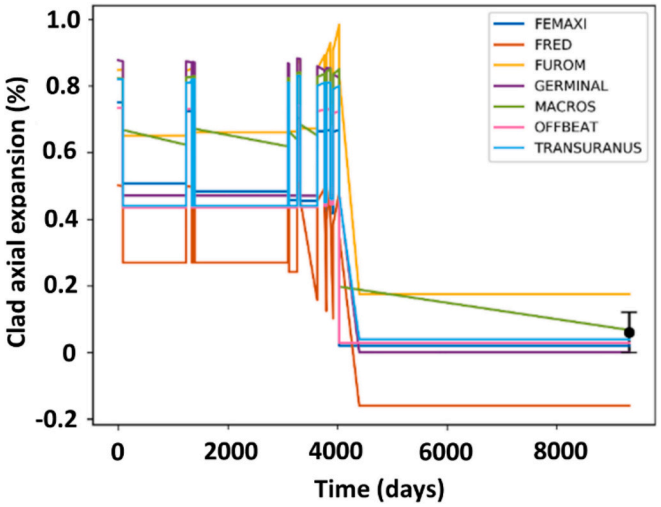


Fig. 5. Evolution of cladding axial expansion over the entire irradiation cycle and storage (colored curves) compared to the experimental data (black dot with experimental uncertainty ±ε).

the irradiation. Firstly, it is evident that only MACROS demonstrates a reduction in cladding expansion during both storage and inter-cycles. This behaviour appears to be directly linked with the cooling period and therefore the thermal regime, a point which will be dedicated to in the discussion section. It has been established that several codes (FUROM, GERMINAL and FRED) predict a reduced cooling rate prior to attaining room temperature during storage. However, this does not appear to exert an influence on the ultimate outcomes. A comparison of the experimental measurement (black dot) with the value calculated at the end of the storage period (curve) reveals that five codes are in good agreement. FRED's estimation of cladding expansion is found to be inaccurate, yielding a negative final value. In this instance, the result suggests a correlation with cooling at ambient temperature.

The observations made on the cladding and the fuel column lengths are indicative of the significance of the thermal regime that is attained during irradiation. This issue will be discussed in more detail subsequently. Furthermore, the potential for enhancement of the relocation model should be given full consideration, as well as the description of the bonding effects between pellets and clad, as previously mentioned.

As described in the introduction, this paper presents the results of the second phase of the benchmark, following the code-to-code comparison phase (Jaramillo-Sierra et al., 2025b). Table 5 summarizes the improvements achieved by code users between the two phases. The "+" symbol indicates an improvement (the simulation result is in better agreement with the EPI), the "-" symbol indicates a deterioration (the simulation result is in less agreement with the EPI), and the "=" symbol means there is no change between the phases. FEMAXI is not listed in the table because it showed no variation between the two phases; the results were identical. A clear improvement can be noted for the plenum pressure and the He and Xe composition of the plenum.

4.2. Pellet scale results

This section is devoted to the local values, which are associated with the pellet scale, and more specifically, the diameters of fuel and cladding. As demonstrated in Table 6, all calculated values have been summarised.

The diameters of both the outer and inner cladding, as calculated by the relevant codes, demonstrate strong agreement with the experimental data. Moreover, Fig. 6(a) illustrates the evolution of the cladding inner diameter along the fuel column at the end of the irradiation. A comparison of GERMINAL, MACROS and FUROM reveals a high degree of similarity in shape, with a local increase in diameter at the Peak Power Node (PPN - axial position where the linear power is at its maximum) (~361.5 mm/ Bottom of Fissile Column (bfc)). However, for MACROS, the maximum appears to be shifted towards the bottom of the column. In the case of FEMAXI, the behaviour is almost flat, while OFFBEAT and TRANSURANUS show a moderated increase at the PPN. Conversely, FRED exhibits a distinctly divergent pattern of behaviour, characterised by a diminution in internal diameter for axial dimensions ranging from 20 to 60 cm.

With regard to the pellet diameters, however, a more challenging comparison can be made. An investigation into the internal radius was conducted, and through the analysis of macrographs of pellets at the PPN and at the top of the column, an off-centered central hole at the PPN was observed (Fayette et al., 2026). Consequently, the experimental value is considered as an average value. With regard to codes, it should be noted that OFFBEAT and GERMINAL are capable of full 3D simulations; however, axisymmetric models were used in the calculations

Table 5
Improvement (+), deterioration (−) or no change (=) between the code-to-code phase (Jaramillo-Sierra et al., 2025b) and this work for the pin scale results.

	FRED	FUROM	GERMINAL	OFFBEAT	TRANSURANUS
Plenum gas pressure	−	+	+	+	+
Plenum composition (He)	+	+	+	+	+
Plenum composition (Xe)	+	−	+	−	+
Plenum composition (Kr)	−	−	+	−	=
Fuel column length	+	=	−	−	+
Clad length	=	−	=	−	=

Table 6
Pellet and cladding diameters calculated by all codes at EOL compared to the PIE values and the fuel central temperature of the fuel calculated at BOC1(with green for data within ±1ε, yellow for data within ±2ε and red for data outside ±2ε).

Radius (cm)	Axial level (mm/bfc)	V-2Ɛ	PIE value	V+2Ɛ	FEMAXI	FRED	FUROM	GERMINAL	OFFBEAT	TRANSURANUS	MACROS
Clad outer	361.5	0.324	0.329	0.334	0.3275	0.3265	0.329	0.328	0.3275	0.3275	0.328
	728.9	0.322	0.328	0.334	0.3275	0.3275	0.328	0.3275	0.3275	0.3275	0.3275
Clad inner	361.5	0.2785	0.2825	0.2865	0.2825	0.2815	0.284	0.283	0.2825	0.2825	0.283
	728.9	0.278	0.282	0.286	0.2825	0.2825	0.283	0.283	0.2825	0.2825	0.2825
Pellet outer	361.5	0.2795	0.282	0.2845	0.2827	0.281	0.279	0.283	0.2828	0.2795	0.2775
	728.9	0.2775	0.27975	0.2825	0.27975	0.2765	0.2775	0.2825	0.27945	0.276	0.278
Central hole	361.5	0.1075	0.11775	0.1285	0.1045	**0.096**	0.111	0.103	0.10785	0.1105	0.118
	728.9	0.101	0.10525	0.11	0.1035	0.102	0.111	0.1035	0.1095	0.1025	0.105
Fuel central temperature (K)	361.5				2130	2135	2132	2126	2172	2259	2032

performed for the benchmark. Consequently, off-centring could not be accounted for. As a preliminary comparison, Fig. 6(b) demonstrates that, at PPN, the codes generally do not align well with the experiment, with the exception of MACROS, which demonstrate good agreement. However, MACROS fails to reproduce the fuel's inner radius at the top of the rod. In general, the utilisation of codes such as TRANSURANUS, OFFBEAT and FUROM yielded satisfactory profiles; however, they have a tendency to underestimate the diameter of the central hole at the PPN. A number of investigations have recently been published concerning the thermal and porosity dynamics of hollow MOX fuel with off-centered pellets under irradiation, using a Finite Element Method (FEM) model implemented via the MFEM library (Jaramillo-Sierra et al., 2025a; Brunetto et al., 2025). It is evident that the prevailing codes generally underestimate the diameter of the central hole. It is hypothesised by FUROM users that the experimental increase in diameter of the central hole is due to the migration of porosities. This process is thermally activated and occurs in a brief timeframe, especially under conditions of high temperature gradient. Furthermore, the central hole off-centering contributes to an increase in temperature of approximately 100 °C, although this is not factored into the model. The modelling of pore migration and fuel restructuring is not homogeneous across codes. In comparison with the initial geometry at room temperature (central hole radius of 0.1 cm), GERMINAL predicts a slight increase of the central hole radius along the fuel stack. However, this code displays a contrasting trend to other codes, predicting lower values at the PPN. FRED produces a similar trend with lower values, effectively predicting a decrease of the central hole radius around the midpoint, even relatively to the initial geometry. The porosity migration is driven by thermally activated phenomena, and this suggests that the thermal regime at the PPN is underestimated. However, it is also important to consider that many simulations tend to overpredict Xe release. Consequently, while the thermal regime may have been underestimated at PPN, there is no evidence that this is the case on a global scale. The thermal regime that has been achieved during the course of the calculations will be discussed in the following section.

A comparison of the fuel-cladding gap with the diameter data is relevant, since it facilitates an understanding of the gap compensation. The PIE values correspond to the average of the fuel-cladding gap measured around the pellet's diameter, which implies a high level of uncertainty. In this instance, the calculated data appear to be in close agreement, as demonstrated in Table 7. A further comparison of the outer fuel diameters and the gaps reveals a strong correlation between diameter and gap size, with larger diameters corresponding to smaller gaps, and vice versa. As illustrated in Fig. 6(d), a comparison is presented of the calculated evolution of the fuel-cladding gap along the fuel column with the experimental data. The majority of the codes (TRANSURANUS, FRED, OFFBEAT and FEMAXI) demonstrate a more pronounced gap at the extremities of the column, whereas at the maximum flux plane the gap has closed or is approaching closure. The manifestation of this phenomenon is subject to variation, contingent upon the specific code employed. In contrast, MACROS, FUROM and GERMINAL demonstrate a modest enhancement in PPN clearance, which is congruent with the observed variation in cladding diameter. It is interesting to note that the results obtained for FEMAXI and OFFBEAT at PPN demonstrate that the pellet OD is larger than the cladding ID. With regard to the aforementioned results, it is evident that the fuel/cladding gap was closed at PPN, and the contact pressure was calculated to be 15 and 1 MPa, respectively. It is evident that the contact condition cannot be verified.

This section is dedicated to the comparison of the code and experimental data at a local scale. This comparison reveals a number of discrepancies, particularly in cases where the phenomena involved were thermally activated. Examples of such phenomena include restructuring and pore migration. Consequently, a dedicated section of the discussion focuses on the analysis of the thermal regime that is attained during the irradiation.

As described in the introduction, this paper presents the results of the second phase of the benchmark, following the code-to-code comparison phase (Jaramillo-Sierra et al., 2025b). Table 8 summarizes the improvements achieved by code users between the two phases. The “+”

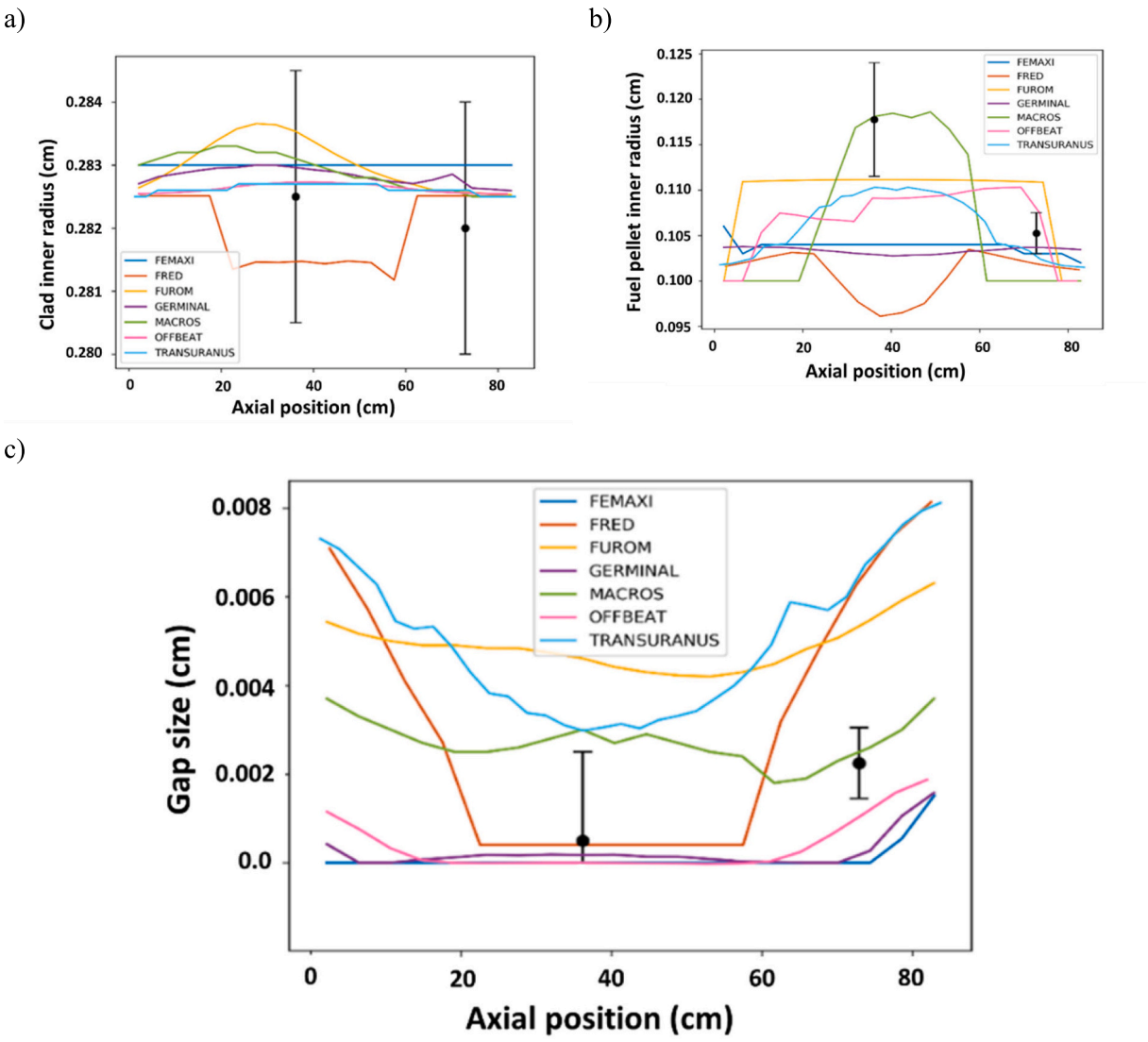


Fig. 6. A) Cladding inner radius b) central hole diameter and c) the gap size along the axial position, at the end of the irradiation calculated (colored curves) and measured values (black dot with experimental uncertainty ±ε).

Table 7
Fuel/cladding gap size at PPN and at the bottom of the column (with green for data within ±1ε, yellow for data within ±2ε and red for data outside ±2ε).

Axial level (mm/bfc*)	V-Ɛ	PIE	V+Ɛ	units	FEMAXI	FRED	FUROM	GERMINAL	OFFBEAT	TRANSURANUS	MACROS
361.5	0	0.0005	0.0025	cm	0	0.0004	0.0046	0.0002	0	0.003	0.003
728.9	0.0015	0.00225	0.0031	cm	0	0.0063	0.0053	0.0001	0.0027	0.0067	0.0022

* Bottom of fissile column.

symbol indicates an improvement (the simulation result is in better agreement with the EPI), the "−" symbol indicates a deterioration (the simulation result is in less agreement with the EPI), and the "=" symbol means there is no change between the phases. FEMAXI is not listed in the table because it showed no variation between the two phases; the results were identical. A clear improvement can be noted for the pellet outer diameters and the gap size.

5. Discussion

As outlined in the previous section, a comparison between codes and post-irradiated experiments reveals several discrepancies. A number of hypotheses have been advanced to explain these discrepancies, including the underestimation of both burn-up and thermal gradient. A detailed discourse on each of these hypotheses is provided in this section.

5.1. Burn-up

The TRIPOLI-4 code was used to calculate the burn-up, which was then compared to the experimental data and the code's prediction (see Fig. 7). All fuel performance calculation codes calculated the burn-up at

Table 8
Improvement (+), deterioration (−) or no change (=) between the code-to-code phase (Jaramillo-Sierra et al., 2025b) and this work for the pellet scale results.

	Axial level (mm/bfc)	FRED	FUROM	GERMINAL	OFFBEAT	TRANSURANUS
Clad outer diameter	361.5	+	=	=	=	=
	728.9	+	=	=	=	=
Clad inner diameter	361.5	+	=	=	+	=
	728.9	+	=	=	+	=
Pellet outer diameter	361.5	+	=	+	+	+
	728.9	+	=	−	+	+
Central hole diameter	361.5	−	=	−	+	+
	728.9	−	=	=	+	+
Gap size	361.5	+	+	−	=	+
	728.9	+	+	−	+	+

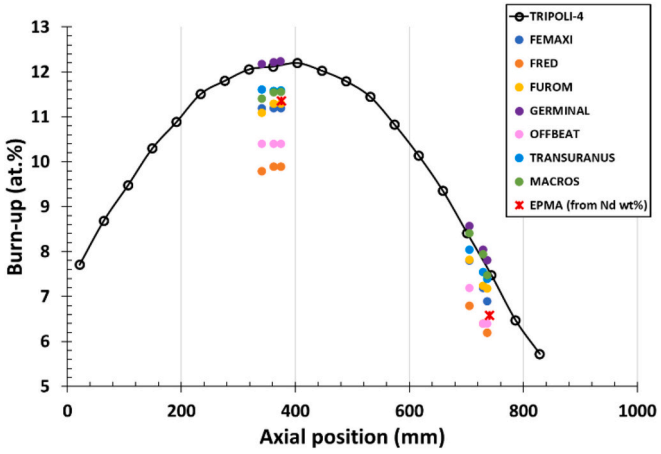


Fig. 7. Burn-up calculated by TRIPOLI-4, all codes and from the Nd (wt%) measured by EPMA (Fayette et al., 2026).

six axial positions, which were close to the experimental measurements: 340.75, 361.5, 374, 704.85, 728.9, 736 mm/bfc. It is evident that the three codes (FRED, OFFBEAT and TRANSURANUS) demonstrate a tendency to underestimate the burn-up for all axial levels. A more detailed examination of the Nd fraction (as a burn-up tracker) measured by Electron Probe Micro Analyses – EPMA - (Fig. 7) reveals that this fission product enables the direct readjustment of the burn-up. As demonstrated in Fig. 7, the experimental data demonstrate a range between 7% and 10% below the data calculated by the TRIPOLI-4 code. Consequently, the burn-up used as the input data appears to be overestimated by around 8–9%. This aspect must therefore be considered in the analysis, as it has a direct impact on the results of the calculations.

5.2. *Thermal fuel behaviour*

The central temperature of the fuel along the column, for all codes, was plotted at BOC1 (Beginning Of Cycle 1) and EOC8 (End of cycle 8) in Fig. 8, corresponding to the beginning and end of life, respectively. The numerical values of the fuel central temperature at PPN and at the BOL are summarised in Table 6. As illustrated in Fig. 8(a), all curves demonstrated a comparable shape, with a maximum attained at PPN. The lowest temperature profile is predicted by MACROS and the highest by TRANSURANUS, showing a maximum central fuel temperature of 2000 and 2250 K, respectively. In contrast, other codes (namely FEMAXI, FRED, FUROM, GERMINAL and OFFBEAT) demonstrate a maximum temperature of 2100 K. The most straightforward explanation for this discrepancy is the specific thermal conductivity law that was used by the codes. In the preliminary sensitivity study, detailed in (Jaramillo-Sierra et al., 2025b), the thermal conductivity laws that were employed are as follows: Philipponneau, Magni et al., EGIFE or a nominal correlation. The use of different thermal conductivity laws between codes would be equivalent to a temperature difference of approximately 100 degrees. Furthermore, the elevation of temperature due to the central hole off-centering (approximately 100 °C) is not considered in this study. At EOC8, a more pronounced variation in behaviour is evident, accompanied by wider gaps in the data. TRANSURANUS, MACROS and FUROM exhibited a shape consistent with that observed at BOC1, with a maximum temperature ranging between 1700 and 1900 K. GERMINAL and FEMAXI attained a temperature of 1550 K at PPN, and for these two codes, a marginal increase in temperature was discernible at the column's top.

In contrast, the final two codes demonstrate divergent shapes: The OFFBEAT code displays a consistent temperature of 1400 K across the entire column, while the FRED code exhibits a maximum at 2100 K at the top of the column and a minimum at PPN of 1950 K. These results demonstrate that from the beginning of life, some temperature differences between codes are observed ($100-200K$), which has a direct impact on the results detailed earlier in this section. To further expand upon this topic, a comparison could be made between the temperatures reached and the temperature thresholds imposed by certain models, such as the Restructuration model. In addition, a comparison of the thermal conductivity laws employed in each code with the experimental measurements conducted on irradiated and fresh CAPRIX fuel would provide a valuable addition to the interpretation of the results obtained.

Nevertheless, a comparison of the fuel-cladding gap size computed by the different codes at different time steps is also of interest. Fig. 8(c) and (d) show the evolution of the gap size along the fuel column at BOC1 and EOC8 respectively. And Fig. 8(e) shows the gap size at PPN throughout the entire irradiation, the time range shown ends at 5000 days to provide better visibility during the irradiation cycles. Firstly, it should be noted that the values of gap size at EOL (End Of Life) provided in Fig. 8(c) and (d) demonstrate that the predictions made by the codes are, in effect, significantly different. As demonstrated in Fig. 8, the same conclusion is drawn. The results for the gap size at BOC1 are largely homogeneous, with the exception of the MACROS, which are nevertheless consistent with the lower temperatures predicted at BOC1. It can thus be concluded that the discrepancy in temperature measurements across the various codes is primarily attributable to variations in fuel thermal conductivity and gap evolution. However, no consistent trend in gap size at EOC8 is observed (see Fig. 8(d)), suggesting that alternative factors may be responsible for the observed temperature discrepancy at EOC8. As demonstrated in Fig. 8(e), these discrepancies are evident throughout the entire irradiation period. From the outset, three distinct groups of code results are evident: one approaching the gap closure (GERMINAL), one approaching 0.0041 cm (FRED, MACROS, OFFBEAT), and the other code results approaching 0.0091 cm. However, these same groupings of results are not systematically found when it comes to temperature, which indicates that other mechanisms are responsible for these discrepancies. This observation is of particular pertinence within the context of the models employed.

6. Conclusions

The objective of the present study is to examine the behaviour of fuel

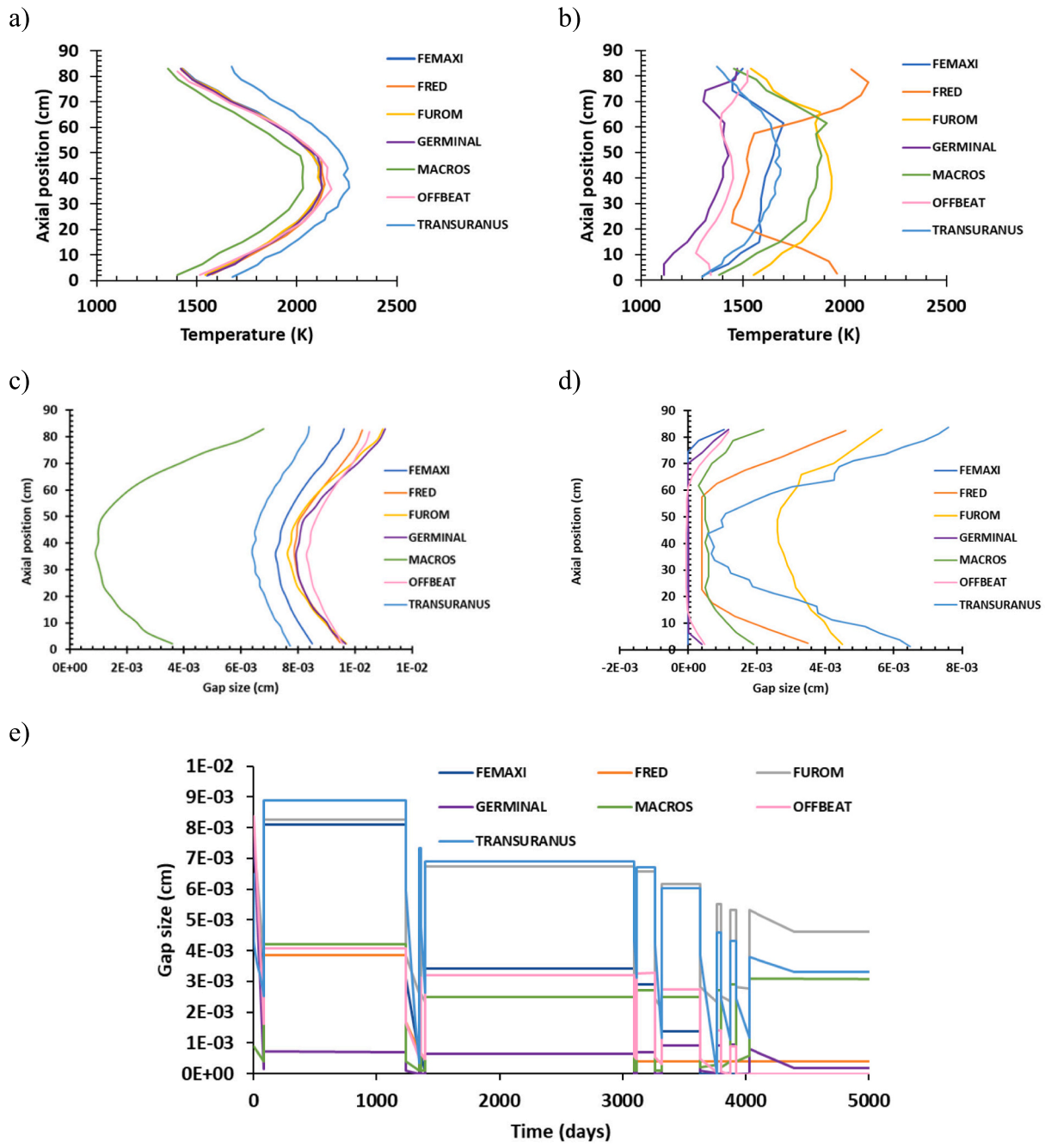


Fig. 8. Fuel central temperature calculated by all codes along the fuel column at different time step of the irradiation a) at BOC1 and b) at EOC8, as well as the fuel-cladding gap size c) at BOC1 d) at EOC8 and e) along the irradiation at PPN.

pins with elevated Pu content when subjected to irradiation in conditions analogous to those of a fast reactor. The analyses were performed by using fuel performance codes to extend their validation domain. In the course of this study, a total of seven codes were subjected to comparative analysis with each other, as well as with the selected post-irradiation experimental data from (Fayette et al., 2026). The primary challenge in this study was to devise a unified methodology for the post-processing of the calculated data across all codes, while also identifying the most effective method for comparing these results. However, despite the application of a common methodology for the codes, inconsistencies between representations were identified, attributable to issues with the post-processing of the calculated data. Notwithstanding this, a detailed analysis was conducted.

As a consequence of a blind comparison (phase 1 of this work described in (Jaramillo-Sierra et al., 2025b)), areas for improvement and optimisation were identified for each of the codes. The comparison yielded a positive result, demonstrating an enhancement in the outcomes. This enhancement enabled a satisfactory simulation of the behaviour of the fuel under irradiation for such elevated Pu contents. It should be noted that, due to the large number of changes made to certain models for each code, it is difficult to conduct a critical analysis to determine which changes had the most significant impact—whether positive or negative—on the comparison between the review and the calculations. It is evident that the comprehensive analysis conducted in this study has enabled the identification of several key points, which are outlined below:

It is imperative that a precise definition of the input data is established in order to enhance the representativeness of the calculations. It

was demonstrated that discrepancies between codes pertaining to external cladding temperature and linear power exerted a direct influence on both global and local results, with the most significant impact being on comparability. Furthermore, the burn-up data calculated by TRIPOLI exhibited a 10% discrepancy with the experimental data (EPMA), which had a direct impact on the calculation results.

The initial part of the study concentrated on the gas data. Section 2.1 details significant discrepancies observed in the production of fission gas. Furthermore, an analysis of the fractional composition of the plenum gas at the end of the product's lifecycle reveals a certain degree of consistency between the codes. It is evident that a potential enhancement to the models could be in the area of low linear power and/or low temperature (for example, during storage or between cycles).

The fuel temperature reached during irradiation varies between the codes. It is imperative to accurately represent this thermal regime, as a number of mechanisms are thermally activated. In order to further investigate the observed temperature dispersions, a comparison of thermal conductivity laws must be considered. Furthermore, the calculated fuel temperatures are found to be significantly influenced by the predicted evolution of the fuel-cladding gap along the irradiation. It was found that the varying rates of gap closure resulted in significant discrepancies in the temperature assessment as the process progressed along the irradiation. In order to provide a comprehensive analysis, a comparison of the models employed to describe the thermally activated physico-chemical phenomena is also necessary. These include pore migration, restructuring and even redistribution models. In the context of the observed discrepancies, certain codes have been identified as areas of potential research, including the diffusion coefficients of U and Pu in the redistribution model. A particular difficulty in reproducing the enlargement of the central hole, its off-centring and the redistribution of actinides and fission products to the PPN was highlighted. One potential future research avenue could involve a refinement of the pore migration model, in addition to the exploration of the central hole off-centering model.

Additionally, the challenges associated with reproducing column expansion were emphasised. The codes suggest that improvements should be made to the relocation model in order to better simulate this phenomenon. The prediction of column expansion is also strongly associated with the modelling of the bonding between fuel and clad.

Notwithstanding the discrepancies observed between the codes and/or the experimental data, the work undertaken in this study has demonstrated the capacity of the codes to optimise and enhance their simulation, with the objective of approximating the PIE. Even if this first qualitative summary addresses a first approach, a more systematic quantitative assessment of the changes in prediction errors between the two phases will be considered in future work. Furthermore, the methodology employed resulted in a comprehensive and analysis, thus facilitating the suggestion of approaches to the development of specific models. This finding thus demonstrates the potential of fuel performance codes modelling pins with high Pu contents.

CRediT authorship contribution statement

M.-M. Desagulier: Writing – review & editing, Writing – original draft, Software, Methodology, Investigation, Formal analysis, Data curation. **D. Jaramillo-Sierra:** Writing – review & editing, Software, Formal analysis, Data curation. **B. Burger:** Writing – review & editing, Software, Formal analysis, Data curation. **L. Argeles:** Writing – review & editing, Formal analysis, Data curation. **M. Stefanowska-Skrodzka:** Supervision, Project administration. **J. Lavarenne:** Supervision, Project administration. **V. Dupont:** Writing – review & editing, Validation, Investigation, Conceptualization. **E. Deveaux:** Software, Formal analysis, Data curation. **A. Del Nevo:** Writing – review & editing, Validation, Supervision, Conceptualization. **E. Brunetto:** Writing – review & editing, Software, Formal analysis, Data curation. **A. Scolaro:** Writing – review & editing, Software, Formal analysis, Data curation. **J. Gado:** Writing – review & editing, Software, Formal analysis, Data curation. **K. Sturm:** Writing – review & editing, Formal analysis, Data curation. **A. Rineiski:** Writing – review & editing, Software, Formal analysis, Data curation. **L. Luzzi:** Writing – review & editing, Software, Formal analysis, Data curation. **A. Magni:** Writing – review & editing, Software, Investigation, Formal analysis, Data curation. **D. Pizzocri:** Writing – review & editing, Software, Formal analysis, Data curation. **K. Mikityuk:** Writing – review & editing, Software, Formal analysis, Data curation. **A. Jiménez-Carrascosa:** Writing – review & editing, Software, Formal analysis, Data curation. **S. Lemehov:** Writing – review & editing, Software, Formal analysis, Data curation. **V. Matocha:** Writing – review & editing, Software, Formal analysis, Data curation. **S. Bebjak:** Writing – review & editing, Software, Formal analysis, Data curation. **C. Strmensky:** Writing – review & editing, Software, Formal analysis, Data curation. **V. Blanc:** Writing – review & editing, Software, Formal analysis, Data curation, Conceptualization. **N. Chauvin:** Visualization, Validation, Supervision, Conceptualization.

Declaration of competing interest

The authors declare that they have no known competing financial interests or personal relationships that could have appeared to influence the work reported in this paper.

Acknowledgment

This work has received funding from the European Union's Horizon 2020 research and innovation program through the PuMMA Project under grant agreement No 945022.

Data availability

Data will be made available on request.

References

Balboa, H., Van Brutzel, L., Chartier, A., Le Bouar, Y., 2017. Assessment of empirical potential for MOX nuclear fuels and thermomechanical properties. J. Nucl. Mater. 495, 67–77. https://doi.org/10.1016/j.jnucmat.2017.07.067.

Brunetto, E.L., Fiorina, C., Pautz, A., van Til, S., Nindiyasari, F., Fedorov, A., Scolaro, A., 2025. Development of a dynamic-mesh porosity transport model for multi-dimensional fuel performance codes. J. Nucl. Mater. 608, 155717. https://doi.org/10.1016/j.jnucmat.2025.155717.

Bruschi, E., Barani, T., 2015. Extension and Validation of a Transient Fission Gas Release Model for the TRANSURANUS Fuel Performance Code. Thèse. Politecnico di Milano. https://www.politesi.polimi.it/handle/10589/115641.

Combette, P., Milet, C., Tanis, G., Crouzet, J., Masson, M., 1977. In-pile creep study on mixed oxide (U, Pu)O2. In: Cundy, M.R., Von der Hardt, P., Loelgen, R.H. (Eds.), Measurement of Irradiation-Enhanced Creep in Nuclear Materials. Elsevier, pp. 37–47. https://doi.org/10.1016/B978-0-7204-0572-9.50009-5.

Fayette, L., Chauvin, N., Lamontagne, J., Blanc, V., Martin, F., Reboul, S., Robert, N., Zacharie-Aubrun, I., Blay, T., Hanifi, K., Roure, I., Bienvenu, P., Noirot, J., 2026. Post-irradiation examinations on a fast reactor MOX fuel pin with high Pu content irradiated at high burnup in PHENIX. J. Nucl. Mater. 619, 156245. https://doi.org/10.1016/j.jnucmat.2025.156245.

Gerschenfeld, A., Gorsse, Y., 2022. Development of a robust multiphase flow solver on general meshes; application to sodium boiling at the subchannel scale. In: NURETH-19 – 19th International Topical Meeting on Nuclear Reactor Thermal Hydraulics. Brussels (Virtual), Belgium.

Herbst, R.S., Baron, P., Nilsson, M., 2011. Standard and advanced separation: PUREX processes for nuclear fuel reprocessing. In: Nash, K.L., Lumetta, G.J. (Eds.), Advanced Separation Techniques for Nuclear Fuel Reprocessing and Radioactive Waste Treatment. Woodhead Publishing, pp. 141–175. https://doi.org/10.1533/9780857092274.2.141.

Jaramillo-Sierra, D., Blanc, V., Barani, T., Cammi, A., Del Nevo, A., 2025a. Off-centering effects on MOX fuel behavior. Nucl. Eng. Des. 444, 114372. https://doi.org/10.1016/j.nucengdes.2025.114372.

Jaramillo-Sierra, D., Stefanowska-Skrodzka, M., Lavarenne, J., Deveaux, E., Brunetto, E., Matocha, V., Magni, A., Sturm, K., Mikityuk, K., Wang, Y., Jiménez-Carrascosa, A., Gado, J., Burger, B., Blanc, V., Dupont, V., Argeles, L., Perrin, B., Michel, G., Scolaro, A., Fiorina, C., Peltonen, J., Del Nevo, A., Luzzi, L., Pizzocri, D., Lemehov, S., Bebjak, S., Chrebet, T., Strmensky, C., 2025b. PuMMA blind benchmark: performance of high plutonium content MOX fuel under irradiation. Nucl. Eng. Des. 435, 113960. https://doi.org/10.1016/j.nucengdes.2025.113960.

Languille, A., Millet, P., Rouault, J., Pillon, S., 1998. Nuclear fuels for actinides burning CAPRA and SPIN programmes status. J. Alloys Compd. 271–273, 517–521. https://doi.org/10.1016/S0925-8388(98)00139-X.

Lavarenne, J., Bubelis, E., Gicquel, S., Krepel, J., Lainet, M., Lindley, B., Mikityuk, K., Murphy, C., Perrin, B., Pfrang, W., Ponomarev, A., Schubert, A., Shwageraus, E., Van Uffelen, P., 2019. A 2-D correlation to evaluate fuel-cladding gap thermal conductance in mixed oxide fuel elements for sodium-cooled fast reactors. Zenodo. https://doi.org/10.5281/zenodo.3541656.

Lemehov, S., Cen, S., 2020. D6.3 – New Correlations of Thermal Expansion and Young's modulus Based on Existing Literature and New Data. INSPYRE deliverable.

NEA (Nuclear Energy Agency), 2025. Recommendations on Fuel Properties for Fuel Performance Codes. OECD Publishing, Paris.

NEA (Nuclear Energy Agency), 2026. The JEFF-3.1.1 Nuclear Data Library. https://www.oecd-nea.org/jcms/pl_36824/the-jeff-3-1-1-nuclear-data-library?details=true (accessed 11 March 2026).

Pastore, G., Luzzi, L., Di Marcello, V., Van Uffelen, P., 2013. Physics-based modelling of fission gas swelling and release in UO_2 applied to integral fuel rod analysis. Nucl. Eng. Des. 256, 75–86. https://doi.org/10.1016/j.nucengdes.2012.12.002.

Philipponneau, Y., 1992. Thermal conductivity of (U, Pu)O_{2-x} mixed oxide fuel. J. Nucl. Mater. 188, 194–197.

Pizzocri, D., Barani, T., Bruschi, E., Luzzi, L., Van Uffelen, P., Pastore, G., 2015. Modelling of burst release in oxide fuel and application to the Transuranus code. In: 11th international conference on WWER fuel performance, modelling and experimental support. Proceedings, pp. 317–326.

Routbort, J.L., Javed, N.A., Voglewede, J.C., 1972. Compressive creep of mixed-oxide fuel pellets. J. Nucl. Mater. 44, 247–259. https://doi.org/10.1016/0022-3115(72)90036-0.

TRIPOLI-4® Project Team, 2015. TRIPOLI-4®, CEA, EDF and AREVA reference Monte Carlo code. Ann. Nucl. Energy 82, 151.

Van Uffelen, P., Schubert, A., Luzzi, L., Barani, T., Magni, A., Pizzocri, D., Lainet, M., Marelle, V., Michel, B., Boer, B., Lemehov, S., Cen, S., Del Nevo, A., 2025. D7.2 – incorporation and verification of models and properties in fuel performance codes. PuMMA deliverable.

Venard, C., Deveaux, E., 2021. D2.1.1: CAPRIX irradiation conditions in Phenix. Livrable de projet, PuMMA project deliverable.